J. Plasma Physics (1999), *vol.* 61, *part* 2, *pp.* 221–240. Printed in the United Kingdom

Magnetohydrodynamic spectrum of gravitating plane plasmas with flow

B. van der HOLST, R. J. NIJBOER and J. P. GOEDBLOED
FOM–Institute for Plasma Physics Rijnhuizen, Edisonbaan 14, Postbus 1207, 3430 BE Nieuwegein, The Netherlands

(Received 22 June 1998 and in revised form 6 October 1998)

The ideal magnetohydrodynamic spectrum of gravitating plane plasmas with equilibrium flow is investigated. Flow makes the spectral problem non-self-adjoint, so that the spectrum can become overstable. The criteria for cluster spectra to appear are derived analytically and both stable and unstable sides of the spectrum are examined numerically. Above certain critical values of the shear flow at the resonant surface, the gravitating interchange modes disappear. However, the local extrema of the continua can then take over the cluster spectrum.

1. Introduction

The analysis of the magnetohydrodynamic (MHD) spectrum of equilibria with flow dates back to the work of Frieman and Rotenberg (1960). However, most of the studies of waves and instabilities of astrophysical and laboratory plasmas have been performed under the assumption of a static equilibrium. Recently, interest in stationary equilibria, as well as their spectral properties, has grown considerably.

In astrophysics, plasma flows play a dominant role, for instance in rotating accretion disks and in collimated jets, such as the jets emitted from radio galaxies, white dwarfs or neutron stars (see e.g. Corbelli and Torricelli-Ciamponi 1989). Another important class of astrophysical phenomena that involve plasma flows, and for which there exist measurements with high spatial resolution, is that of coronal flux tubes. These flux tubes may be responsible for the heating of the solar corona. Furthermore, much work has been done on the Kelvin–Helmholtz instability of the velocity shear layers between magnetospheres of planets and the solar wind, or between streams of different velocities in the solar wind itself (Miura and Pritchett 1982; Gonzáles and Gratton 1994).

In fusion research, the problem of rotating plasma equilibria has attracted increasing attention over the years (Bondeson et al. 1987; Chu et al. 1995), because of the significant rotating plasma flow induced by neutral-beam injection or a divertor. Both are important for future steady-state advanced tokamaks.

In this paper, we discuss the effect of shear flow on both stable and unstable cluster spectra of a gravitating plane plasma slab. In Sec. 2, the eigenvalue problem is stated for the Lagrangian displacement. In Sec. 3, we examine the singularities of the differential equation derived. This leads to the description of the classical flow and MHD continua and clustering to their local extrema. In Sec. 4, we look into the effect of shear flow on gravitational interchange modes clustering to the

resonant surface. The numerical results are discussed in Sec. 5. Finally, conclusions are drawn in Sec. 6.

2. Eigenvalue problem

In this section, the eigenvalue problem is derived for a gravitating plane plasma slab contained between two perfectly conducting walls. First, the basic formulation of Frieman and Rotenberg is recalled (Sec. 2.1). Then, the equation of motion is reduced to a coupled system of first-order differential equations for a gravitational plane slab (Sec. 2.2). Finally, the equivalent second-order formulation is discussed (Sec. 2.3).

2.1. Frieman and Rotenberg formulation

As shown by Frieman and Rotenberg (1960), the motion of the Lagrangian displacement $\boldsymbol{\xi}$ of a fluid element is given by

$$\rho\frac{\partial^2\boldsymbol{\xi}}{\partial t^2} + 2\rho\mathbf{v}\cdot\boldsymbol{\nabla}\frac{\partial\boldsymbol{\xi}}{\partial t} - \mathbf{F}(\boldsymbol{\xi}) = 0, \tag{2.1}$$

where

$$\mathbf{F}(\boldsymbol{\xi}) = -\boldsymbol{\nabla}\Pi + \mathbf{B}\cdot\boldsymbol{\nabla}\mathbf{Q} + \mathbf{Q}\cdot\boldsymbol{\nabla}\mathbf{B} - \mathbf{g}\boldsymbol{\nabla}\cdot(\rho\boldsymbol{\xi}) + \boldsymbol{\nabla}\cdot\left[\rho\boldsymbol{\xi}(\mathbf{v}\cdot\boldsymbol{\nabla})\mathbf{v} - \rho\mathbf{v}\mathbf{v}\cdot\boldsymbol{\nabla}\boldsymbol{\xi}\right]. \tag{2.2}$$

Here

$$\mathbf{Q} = \boldsymbol{\nabla}\times(\boldsymbol{\xi}\times\mathbf{B}) \tag{2.3}$$

is the Eulerian perturbation of the magnetic field,

$$\Pi = -\boldsymbol{\xi}\cdot\boldsymbol{\nabla}p - \gamma p\boldsymbol{\nabla}\cdot\boldsymbol{\xi} + \mathbf{B}\cdot\mathbf{Q} \tag{2.4}$$

is the Eulerian perturbation of the total pressure, ρ, $\mathbf{v}$, $\mathbf{B}$ and p are the equilibrium density, plasma flow, magnetic field and kinetic pressure respectively, and $\mathbf{g}$ is the acceleration due to gravity (Berge 1997). The latter is assumed to be constant. As pointed out by Frieman and Rotenberg (1960), for an ideal plasma confined within a perfectly conducting wall, the operators $i\mathbf{v}\cdot\boldsymbol{\nabla}$ and $\rho^{-1}\mathbf{F}$ of (2.1) are symmetric with respect to the inner product $\langle\boldsymbol{\xi}_1,\boldsymbol{\xi}_2\rangle = \frac{1}{2}\int\rho\boldsymbol{\xi}_1^*\cdot\boldsymbol{\xi}_2\,d^3\mathbf{x}$. If we consider normal modes, this implies that if $\omega=\alpha$ is an eigenvalue then $\omega=\alpha^*$ is also an eigenvalue.

2.2. Gravitational plane slab

We shall specialize (2.1) to a plane gravitating plasma slab, infinite in the y and z directions, and contained between two perfectly conducting plates at $x=0$ and $x=1$. The equilibrium is assumed to depend only on the x direction:

$$\rho=\rho(x), \qquad \mathbf{B} = B_y(x)\mathbf{e}_y + B_z(x)\mathbf{e}_z, \qquad \mathbf{g} = -g\mathbf{e}_x, \tag{2.5a}$$

$$p=p(x), \qquad \mathbf{v} = v_y(x)\mathbf{e}_y + v_z(x)\mathbf{e}_z. \tag{2.5b}$$

The only restriction on these quantities is force balance:

$$(p+\tfrac{1}{2}B^2)' = -\rho g, \tag{2.6}$$

where the prime indicates differentiation with respect to x.

Because of the symmetry of the equilibrium, we shall choose normal-mode solutions of the form

$$\boldsymbol{\xi}(x,y,z,t) = (\xi_x(x),\xi_y(x),\xi_z(x))e^{i(k_y y+k_z z-\omega t)}. \tag{2.7}$$

Furthermore, we exploit a field-line projection with unit vectors

$$\mathbf{e}_x = \boldsymbol{\nabla} x, \qquad \mathbf{e}_\perp \equiv \mathbf{e}_\parallel \times \mathbf{e}_x, \qquad \mathbf{e}_\parallel \equiv \frac{\mathbf{B}}{B}. \tag{2.8}$$

In this projection, the gradient acting on perturbed scalar quantities can be written as

$$\boldsymbol{\nabla} = \mathbf{e}_x \frac{\partial}{\partial x} + \mathbf{e}_\perp \frac{iG}{B} + \mathbf{e}_\parallel \frac{iF}{B}, \tag{2.9}$$

where

$$G \equiv -i\mathbf{B} \times \mathbf{e}_x \cdot \boldsymbol{\nabla} = k_y B_z - k_z B_y, \tag{2.10a}$$

$$F \equiv -i\mathbf{B} \cdot \boldsymbol{\nabla} = k_y B_y + k_z B_z, \tag{2.10b}$$

and

$$\frac{F^2 + G^2}{B^2} = k^2 = k_y^2 + k_z^2.$$

We also project the displacement vector $\boldsymbol{\xi}$:

$$\xi \equiv \mathbf{e}_x \cdot \boldsymbol{\xi} = \xi_x, \tag{2.11a}$$

$$\eta \equiv i\mathbf{e}_\perp \cdot \boldsymbol{\xi} = \frac{i}{B}(B_z \xi_y - B_y \xi_z), \tag{2.11b}$$

$$\zeta \equiv i\mathbf{e}_\parallel \cdot \boldsymbol{\xi} = \frac{i}{B}(B_y \xi_y + B_z \xi_z), \tag{2.11c}$$

where the factors i have been inserted such that the final expressions are real in the corresponding static case.

By using (2.5)–(2.11), (2.1) can be recast as a coupled system of first-order differential equations describing the equation of motion:

$$AS \begin{pmatrix} \xi' \\ \Pi' \end{pmatrix} + \begin{pmatrix} C & D \\ E & -C \end{pmatrix} \begin{pmatrix} \xi \\ \Pi \end{pmatrix} = 0, \tag{2.12}$$

where the prime indicates the derivative with respect to x. This formulation is the gravitational analogue with flow of that obtained by Appert et al. (1974) for the static cylindrical equilibrium. Here, the coefficients are given by

$$A = \rho\tilde{\omega}^2 - F^2, \tag{2.13a}$$

$$S = (\gamma p + B^2)(\rho\tilde{\omega}^2 - F^2 M_c^2), \tag{2.13b}$$

$$C = -\rho g \rho \tilde{\omega}^2 A, \tag{2.13c}$$

$$D = \rho^2 \tilde{\omega}^4 - k^2 S, \tag{2.13d}$$

$$E = -AS(A + \rho' g) - \rho^2 g^2 A^2, \tag{2.13e}$$

where the ratio of the cusp to the Alfvén speed,

$$M_c = \frac{v_c}{v_A} = \left(\frac{\gamma p}{\gamma p + B^2}\right)^{1/2}, \tag{2.14}$$

is called the cusp Alfvén Mach number and

$$\tilde{\omega} \equiv \omega - \mathbf{k} \cdot \mathbf{v} = \omega - k_y v_y - k_z v_z \tag{2.15}$$

is the frequency in a locally (at some x) comoving frame. Furthermore, the perpendicular and parallel tangential components of the displacement vector $\boldsymbol{\xi}$ are

expressed by

$$\eta = -\frac{G}{BA}\Pi, \tag{2.16a}$$

$$\zeta = -\frac{F}{BS}(\gamma p\Pi + B^2\rho g\xi). \tag{2.16b}$$

Expressing these compononents in terms of ξ' and ξ by using (2.12) introduces a division by D, which has been the source of much confusion (see below).

2.3. Equivalent formulation

The formulation in two dependent variables as in (2.12) can be reduced to one second-order equation. Here we choose ξ as the dependent variable, and obtain

$$\left[\frac{AS}{D}\xi'\right]' + \left[U + \frac{V}{D} + \left(\frac{W}{D}\right)'\right]\xi = 0. \tag{2.17}$$

This equation was first derived by Goedbloed (1971) for the static equilibrium case. With flow, the only – but extremely important – change is the replacement of ω by $\tilde{\omega}$. The coefficients are given by

$$U = A + \rho' g, \tag{2.18a}$$

$$V = -k^2\rho^2 g^2 A, \tag{2.18b}$$

$$W = C = -\rho g\rho\tilde{\omega}^2 A. \tag{2.18c}$$

The coefficients C, D and E of the first-order system (2.12) have the special property that the determinant of the second term is proportional to AS:

$$C^2 + DE = -[(A + \rho' g)D - k^2\rho^2 g^2 A]AS. \tag{2.19}$$

This guarantees that the Alfvén and slow singularities are regular, which is obvious from the second-order formulation. On the other hand, the coefficients V and W of the second-order differential equation (2.17) also satisfy a special property, namely

$$W^2 + ASV = \rho^2 g^2 A^2 D. \tag{2.20}$$

This guarantees that the zeros of D are apparent singularities, which is obvious from the first-order formulation. The two properties (2.19) and (2.20) are unrelated.

The first-order formulation (2.12) and the second-order formulation (2.17) are presented here for the gravitating plane slab with flow. The original first-order representation for cylindrical plasmas without flow (Appert et al. 1974) was instrumental in disproving the claim that the $D = 0$ singularities represent continuous spectra (Grad 1973). The cylindrical counterpart of the property (2.19) was derived by Bondeson et al. (1987). The cylindrical counterpart of the property (2.20) is crucial for the demonstration that the initial-value problem is well posed when $D = 0$ (another proof that these are not continuous spectra). This was derived by Goedbloed (1974, 1998).

Equations (2.12) or (2.17) have to be supplemented with boundary conditions in order to close the system. For a rigid wall at the plasma boundary the appropriate conditions are

$$\xi(0) = \xi(1) = 0, \tag{2.21}$$

expressing that there is no displacement perpendicular to the wall. This boundary value problem is converted into a spatial initial-value problem, for example by

fixing $\xi(0)$ and $\Pi(0)$, or $\xi(0)$ and $\xi'(0)$, which is solved iteratively by shooting for the complex eigenvalue ω. Note that, for a plane slab, the equilibrium flow does not show up in the force balance (2.6), and it enters the equations of motion (2.12) and (2.17) only through a Doppler shift of the frequency. Hence the spectral analysis of the gravitational plane plasma slab permits a more transparent analysis of the different singularities than that of a cylindrical plasma.

3. Local analysis of the singularities

In this section we discuss the singularities of the eigenvalue problem (2.17). Since (2.17) does not contain irregular singularities we can use the method of Frobenius to examine the local behaviour of the occurring regular ones. This leads to the distinction between quite different types of singularities associated with different physical effects: the classical Alfvén and slow continua are described by simple zeros of the factor AS (Sec. 3.1); on the other hand, the zeros of D do not yield continua (Sec. 3.2), the classical flow continuum is associated with a quadratic zero in $\tilde{\omega}^2$ (Sec. 3.3), and cluster points may occur when the factor AS develops a quadratic zero (Sec. 3.4).

3.1. Alfvén and slow continua

We first consider the case where the factor AS of (2.17) has a simple zero at $x = x_s$, i.e. $(AS)(x_s) = 0$ and $(AS)'(x_s) \neq 0$. This zero in AS can either mean $A = 0$, resulting from the Alfvén continuum frequency

$$\Omega_A^{\pm}(x) = \Omega_0(x) \pm \omega_A(x), \qquad \Omega_0 \equiv \mathbf{k} \cdot \mathbf{v}, \qquad \omega_A \equiv \frac{F}{\rho^{1/2}}, \tag{3.1}$$

or $S = 0$, resulting from the slow magnetoacoustic continuum frequency

$$\Omega_S^{\pm}(x) = \Omega_0(x) \pm \omega_S(x), \qquad \omega_S = M_c \omega_A. \tag{3.2}$$

Note that the well-known Alfvén and slow continua $\pm\omega_A(x)$ and $\pm\omega_S(x)$ of the static MHD are now extended with an additional x-dependent part $\Omega_0(x)$ due to the flow. Furthermore, we can rewrite A and S as

$$A = \rho(\omega - \Omega_A^-)(\omega - \Omega_A^+), \tag{3.3}$$

$$S = \rho(\gamma p + B^2)(\omega - \Omega_S^-)(\omega - \Omega_S^+), \tag{3.4}$$

showing their dependence on the Doppler-shifted continuum frequency.

The improper eigenfunctions associated with the continua are obtained by expanding the coefficients of (2.17) in $s \equiv x - x_s$ and substituting the leading-order term of the Frobenius expansion, $\xi \propto s^n$, so that we obtain the indicial equation $n^2 = 0$. This implies that the functional form of the displacement ξ of the fluid in the x direction is the same as in the static case for $\omega \to \pm\omega_A$ or $\pm\omega_S$:

$$\xi = u(x)[\ln |s| + \lambda H(s)] + v(x). \tag{3.5}$$

Here H denotes the Heaviside function, λ is an arbitrary constant, and u and v are analytic functions containing two other constants of integration. Therefore the solution (3.5) can always satisfy the boundary conditions. The dominant, non-square-integrable part of the eigenfunctions resides in one of the tangential components η

and ζ. Application of (2.16) gives

$$\eta \approx \mathscr{P}\frac{1}{s} + \lambda\delta(s) \tag{3.6}$$

for the Alfvén waves and

$$\zeta \approx \mathscr{P}\frac{1}{s} + \lambda\delta(s) \tag{3.7}$$

for the slow magnetoacoustic waves. Here $\mathscr{P}$ indicates that the Cauchy principal value is to be taken.

3.2. Apparent singularities

For the discussion of the structure of the spectrum, it is useful at this point to consider the apparent singularities $D = 0$. The expression D can be factored by introducing the local magnetosonic turning-point frequencies

$$\omega^2_{s0,f0} = \frac{1}{2\rho}k^2(\gamma p + B^2)\left\{1 \pm \left[1 - \frac{4\gamma p F^2}{k^2(\gamma p + B^2)^2}\right]^{1/2}\right\}, \tag{3.8}$$

giving rise to the Doppler-shifted frequencies

$$\Omega^{\pm}_{s0}(x) = \Omega_0(x) \pm \omega_{s0}(x), \tag{3.9a}$$

$$\Omega^{\pm}_{f0}(x) = \Omega_0(x) \pm \omega_{f0}(x). \tag{3.9b}$$

By means of the quantities defined in (3.1), (3.2), (3.8) and (3.9), the factor in front of the highest derivative may now be written as

$$\frac{AS}{D} = (\gamma p + B^2)\frac{(\omega - \Omega^-_A)(\omega - \Omega^-_S)(\omega - \Omega^+_S)(\omega - \Omega^+_A)}{(\omega - \Omega^-_{f0})(\omega - \Omega^-_{s0})(\omega - \Omega^+_{s0})(\omega - \Omega^+_{f0})}. \tag{3.10}$$

Whereas the numerator quantities $\{\Omega^{\pm}_A\}$ and $\{\Omega^{\pm}_S\}$ correspond to the continuous spectrum, the denominator quantities $\{\Omega^{\pm}_{f0}\}$ and $\{\Omega^{\pm}_{s0}\}$ do not yield continua. However, they play an important role as separators of the different subspectra, as is evident from the following sequence of inequalities:

$$-\infty \leqslant \Omega^-_{f0} \leqslant \Omega^-_A \leqslant \Omega^-_{s0} \leqslant \Omega^-_S \leqslant \Omega_0 \leqslant \Omega^+_S \leqslant \Omega^+_{s0} \leqslant \Omega^+_A \leqslant \Omega^+_{f0} \leqslant \infty, \tag{3.11}$$

which holds for fixed x. Inhomogeneity causes these frequencies to become extended domains, which may overlap, have maxima and minima, etc., so that a huge variety of spectral structures is possible. Clearly, to simplify the analysis one should first study weakly inhomogeneous plasmas where these frequency ranges are well separated.

Note the important difference with the static MHD spectral structures, where the eigenvalue parameter only appears squared, so that positive and negative freqencies appear in a completely symmetric fashion. Whereas the frequencies (3.11) at fixed x are still symmetric with respect to the central flow frequency Ω_0, this symmetry is completely lost when the collection of frequencies over the interval $0 \leqslant x \leqslant 1$ is considered in the presence of inhomogeneity.

3.3. Flow continua

In Sec. 3.1, the generic case of gravitating plasma with shear flow and magnetic shear was considered. This analysis needs further development when $F = 0$. This condition may arise when a resonant surface is present in plasmas with magnetic shear. This situation will be treated in Sec. 4.1. In the absence of magnetic shear,

the condition $F = 0$ can be satisfied on the whole plasma domain. In that case, the seven innermost frequencies of the inequalities (3.11) collapse onto the single frequency $\mathbf{\Omega}_0$. Then we actually enter the regime of hydrodynamics (modified by the pressure of compressional magnetic effects), and (2.17) reduces to

$$\left[\frac{(\gamma p + B^2)\rho\tilde{\omega}^2}{\rho\tilde{\omega}^2 - k^2(\gamma p + B^2)}\xi'\right]' + \left\{\rho\tilde{\omega}^2 + \rho' g - \frac{k^2\rho^2 g^2}{\rho\tilde{\omega}^2 - k^2(\gamma p + B^2)} - \left(\frac{\rho g \rho\tilde{\omega}^2}{\rho\tilde{\omega}^2 - k^2(\gamma p + B^2)}\right)'\right\}\xi = 0. \quad (3.12)$$

Hence we obtain a continuum singularity $\omega = \mathbf{\Omega}_0(x) \equiv \mathbf{k}\cdot\mathbf{v}$ when there is a quadratic zero $\tilde{\omega}^2 = 0$.

The pure hydrodynamical case ($B = 0$) was analysed by Case for the incompressible limit ($\gamma p \to \infty$) both without gravity (Case 1960a) and with gravity for an exponential atmosphere (Case 1960b). To the best of our knowledge, he was the first author to introduce the flow continuum $\{\mathbf{\Omega}_0\}$ and to analyse its consequences. The transformation to the Eulerian formulation, exploited by Case, involves the introduction of the vertical flow velocity $u = -i\tilde{\omega}\xi$. The fact that this transformation once more brings in the singular factor $\tilde{\omega}$ should not be confused with the flow continuum itself, which is present in both the Lagrangian and Eulerian formulations. This point is elaborated elsewhere (Goedbloed et al. 1999).

The extension with compressibility, described by (3.12), does not change the flow continuum, but it introduces additional terms affecting the cluster spectra. Moreover, it introduces a denominator

$$\rho\tilde{\omega}^2 - k^2(\gamma p + B^2) = \rho(\omega - \mathbf{\Omega}_{f0}^-)(\omega - \mathbf{\Omega}_{f0}^+)$$

that may vanish on the interval. This gives rise to apparent singularities of the same kind as encountered in the MHD case when $D \to 0$, so that they do not correspond to continuous spectra here either. This special feature of the hydrodynamic limit has been highlighted by Goedbloed (1974, 1998) in the construction of the resolvent operator mentioned in Sec. 2.3.

When there is a quadratic zero $\tilde{\omega}^2(x_s) = 0$, to lowest order in $s = x - x_s$, (3.12) reduces to

$$(s^2\xi')' + D_0\xi = 0, \quad (3.13)$$

where

$$D_0 = -\frac{k^2}{\rho\mathbf{\Omega}_0'^2}\left(\rho' g + \frac{\rho^2 g^2}{\gamma p + B^2}\right). \quad (3.14)$$

By substituting the leading-order term of the Frobenius expansion, $\xi \propto s^n$, one obtains the indicial equation $n(n+1) + D_0 = 0$ with roots $n_{1,2} = -\frac{1}{2} \pm (\frac{1}{4} - D_0)^{1/2}$. When $D_0 < \frac{1}{4}$, the indices are real, and one of them ($n_1 > -\frac{1}{2}$) represents the 'small' solution, whereas the other ($n_2 < -\frac{1}{2}$) represents the large solution. Here large and small are to be understood in the sense of Newcomb's (1960) analysis for the static equilibrium case. Exploiting the quadratic form of the potential energy, he demonstrated that the small solution may jump at the singularity, whereas the large one should be continuous. This analysis carries over to the present case. Consequently, boundary conditions can always be satisfied, and $\omega \in \{\mathbf{\Omega}_0(x)\}$ is part of the continuous spectrum.

When $D_0 > \frac{1}{4}$, the indices are complex, and the solutions oscillate infinitely

rapidly as the singularity is approached:

$$\xi_1 = |s|^{-1/2}\cos(\sigma \ln|s|), \qquad \xi_2 = |s|^{-1/2}\sin(\sigma \ln|s|), \tag{3.15}$$

$$\sigma = (D_0 - \tfrac{1}{4})^{1/2}. \tag{3.16}$$

These 'improper' eigenfunctions can be made to satisfy the boundary conditions by an arbitrarily small adjustment. Hence any $\omega \in \{\Omega_0(x)\}$ is again part of the continuous spectrum. Moreover, endpoints of $\Omega_0(x)$, where $\Omega_0'(x) \neq 0$, in the interval $0 \leqslant x \leqslant 1$ are cluster points of discrete spectra outside the flow continuum. A generic example has been studied by Case (1960b) and Dyson (1960) for the incompressible exponential atmosphere, stretching out from $x = 0$ to ∞. They find a flow continuum $0 \leqslant \omega \leqslant \infty$ and a spectrum of discrete modes $\omega_n < 0$ clustering to 0. The condition $D_0 > \frac{1}{4}$ for a cluster spectrum in the hydrodynamic case takes the form of a competition between Rayleigh–Taylor terms and shear flow:

$$\rho' g + \frac{\rho^2 g^2}{\gamma p + B^2} < -\frac{1}{4}\frac{\rho \Omega_0'^2}{k^2}, \tag{3.17}$$

We return to the physical implications in Sec. 5.2.

3.4. Local extrema of the MHD continua and clustering

In Sec. 3.1, we examined the case where the factor AS has a simple zero. Now, we shall consider situations where AS develops a quadratic zero at $x = x_s$. First, we consider the Alfvén factor

$$A = \rho(\tilde{\omega}^2 - w_A^2) = \rho(\omega - \Omega_A^-)(\omega - \Omega_A^+)$$

for non-vanishing $\tilde{\omega}$ (the case of resonant surfaces with simultaneous zeros of $\tilde{\omega}$ and ω_A will be discussed in Sec. 4.2). The Alfvén factor yields

$$\omega = \Omega_A^{\pm}(x_s) \neq \Omega_0(x_s), \qquad \Omega_A^{\pm\prime}(x_s) = 0, \qquad \Omega_A^{\pm\prime\prime}(x_s) \neq 0, \tag{3.18}$$

so that we are looking at a local extremum in either one of the Doppler-shifted Alfvén continua $\Omega_A^{\pm}$.

To lowest order in $s = x - x_s$, (2.17) reduces to

$$(s^2\xi')' + D_A\xi = 0, \tag{3.19}$$

where

$$D_A = -\frac{G^2}{B^2}\frac{2\rho' g}{A''}, \tag{3.20}$$

and $A'' = \mp 2\rho\omega_A(\Omega_A^{\pm})''$. By substituting the leading-order term of the Frobenius expansion, $\xi \propto s^n$, we obtain the indicial equation $n(n+1) + D_A = 0$, with solutions $n_{1,2} = -\frac{1}{2} \pm i\sigma$, where $\sigma = (D_A - \frac{1}{4})^{1/2}$. These indicial exponents are complex if $D_A > \frac{1}{4}$, so that wildly oscillating solutions are obtained:

$$\xi_1 = |s|^{-1/2}\cos(\sigma \ln|s|), \qquad \xi_2 = |s|^{-1/2}\sin(\sigma \ln|s|). \tag{3.21}$$

In analogy to the analysis by Case (1960b) and Dyson (1960), this implies that if

$$\frac{G^2}{B^2}\rho' g > \pm\frac{1}{4}\rho\omega_A(\Omega_A^{\pm})'' > 0 \tag{3.22}$$

at a local minimum of Ω_A^+ (or a maximum of Ω_A^-), then a cluster spectrum of discrete

modes just below the continuum Ω_A^+ (or above Ω_A^-) is to be expected. Vice versa, if

$$\frac{G^2}{B^2}\rho' g < \pm\tfrac{1}{4}\rho\omega_A(\Omega_A^\pm)'' < 0 \tag{3.23}$$

at a local maximum of Ω_A^+ (or a minimum of Ω_A^-) then a cluster spectrum of discrete modes just above the continuum Ω_A^+ (or below Ω_A^-) is to be expexted.

In the static case, the above considerations lead to a Sturmian spectrum in the real eigenvalue ω^2 (the number of nodes in the eigenfunctions increases with ω^2) of discrete modes clustering to the local extremum when the condition (3.22) is satisfied, and to an anti-Sturmian cluster spectrum in the case of criterion (3.23) (Goedbloed 1984). Furthermore, as pointed out by Bondeson et al. (1987), if the frequency of the local extremum of the Alfvén continuum coincides with some other continuum modes then the cluster spectrum may become overstable. The sequences of discrete cluster modes may also disappear. However, real cluster spectra in equilibria satisfying the inequalities (3.22) and (3.23) can always be constructed by considering inhomogeneities that are weak enough for the continua to be well-separated. This is possible by virtue of the set of inequalities (3.11).

A similar analysis can be carried out for a quadratic zero of the slow factor

$$S = \rho(\gamma p + B^2)(\tilde{\omega}^2 - \omega_S^2) = \rho(\gamma p + B^2)(\omega - \Omega_S^-)(\omega - \Omega_S^+)$$

for non-vanishing $\tilde{\omega}$:

$$\omega = \Omega_S^\pm(x_s) \neq \Omega_0(x_s), \qquad \Omega_S^{\pm\prime}(x_s) = 0, \qquad \Omega_S^{\pm\prime\prime}(x_s) \neq 0. \tag{3.24}$$

Hence we are looking at a local extremum in either one of the Doppler-shifted slow continua $\Omega_S^\pm$. Oscillatory solutions and cluster spectra are to be expected when

$$\frac{k^2\rho^2 g^2}{\gamma p + B^2} + \frac{M_c^4 F^2}{B^2}\left(\frac{\rho g}{M_c^2}\right)' - \frac{M_c^4 F^4}{\gamma p + B^2} > \pm\tfrac{1}{4}\rho\omega_S(\Omega_S^\pm)'' > 0 \tag{3.25}$$

at a local minimum of Ω_S^+ (or a maximum of Ω_S^-), and

$$\frac{k^2\rho^2 g^2}{\gamma p + B^2} + \frac{M_c^4 F^2}{B^2}\left(\frac{\rho g}{M_c^2}\right)' - \frac{M_c^4 F^4}{\gamma p + B^2} < \pm\tfrac{1}{4}\rho\omega_S(\Omega_S^\pm)'' < 0 \tag{3.26}$$

at a local maximum of Ω_S^+ (or a minimum of Ω_S^-).

The criteria (3.25) and (3.26) depend on the magnitude of the wavenumbers k_y and k_z. When $|F|$ is small, the first term in (3.25) and (3.26) is dominant, so that cluster spectra can only appear at a local minimum of Ω_S^+ or at a local maximum of Ω_S^- when the inequality (3.25) is satisfied. On the other hand, in the short-wavelength limit, the third term in (3.25) and (3.26) is dominant. Then only the condition (3.26) can be satisfied.

4. Gravitational interchange modes

In Sec. 3, we studied cases with a simple or quadratic zero of the factor AS. This led to the description of the MHD continua and clustering to their local extrema. However, when there is a resonant surface ($F = 0$, $F' \neq 0$), the four slow and Alfvén frequencies coincide with Ω_0, so that AS develops a fourth-order zero. It is obvious from the set of inequalities (3.11) that the slow turning-point frequencies then also coincide with Ω_0, so that D develops a second-order zero cancelling two of the zeros

of AS. In effect, the factor AS/D then again has a second-order zero, as in Sec. 3.4, but it is clear that the physical situation is quite different. It corresponds to the possible appearance of gravitational interchanges (Sec. 4.1). Moreover, the assumption of weak inhomogeneity, which was made in Sec. 3 to separate the continua, can no longer be made, since the continua necessarily overlap when there is a resonant surface. Although the resonant surface will be stable above certain critical values of the shear flow, it will be shown that the local extrema of the continua can take over the cluster spectrum in that case (Sec. 4.2).

4.1. Cluster condition

From the static case, it is known (Suydam 1959) that a resonant surface ($F = 0$, $F' \neq 0$) may become locally unstable. If flow is included, according to (3.1) and (3.2), the four continua then coincide at the Doppler-shifted frequency $\omega = \mathbf{\Omega}_0(x_s)$ of the resonant surface. Expansion about the point $x = x_s$ is facilitated by the introduction of the shear Alfvén Mach number

$$M = \frac{\tilde{\omega}'}{\omega_A'} = -\frac{\rho^{1/2}\mathbf{\Omega}_0'}{F'} = -\rho^{1/2}\frac{(\mathbf{k}\cdot\mathbf{v})'}{(\mathbf{k}\cdot\mathbf{B})'}, \tag{4.1}$$

which represents the shear of the flow with respect to the shear of the magnetic field. The different factors of AS and D then become:

$$\omega - \mathbf{\Omega}_S^{\pm} \approx \frac{F'}{\rho^{1/2}}(M \mp M_c)s, \tag{4.2a}$$

$$\omega - \mathbf{\Omega}_{s0}^{\pm} \approx \frac{F'}{\rho^{1/2}}(M \mp M_c)s, \tag{4.2b}$$

$$\omega - \mathbf{\Omega}_A^{\pm} \approx \frac{F'}{\rho^{1/2}}(M \mp 1)s, \tag{4.2c}$$

$$\omega - \mathbf{\Omega}_{f0}^{\pm} \approx \mp k\left(\frac{\gamma p + B^2}{\rho}\right)^{1/2}, \tag{4.2d}$$

so that (2.17) transforms to

$$(s^2\xi')' + D_I\xi = 0, \tag{4.3}$$

where

$$D_I = \frac{k^2}{F'^2}\left(\frac{\rho' g}{1-M^2} + \frac{\rho^2 g^2}{\gamma p + B^2}\frac{1}{M_c^2 - M^2}\right). \tag{4.4}$$

Hence clustering of gravitational interchanges occurs for

$$\rho' g\frac{1}{1-M^2} + \frac{\rho^2 g^2}{\gamma p}\frac{M_c^2}{M_c^2 - M^2} > \frac{1}{4}\frac{F'^2}{k^2}. \tag{4.5}$$

The condition (4.5) is a generalization with flow of the condition for a static plane plasma slab obtained by Newcomb (1961). The cylindrical counterpart is called the Suydam criterion (Suydam 1959), and its modification with flow was obtained by Hameiri (1981). In the static case, when (4.5) is satisfied, an infinite number of unstable discrete gravitational interchange modes will appear, clustering to the marginal point $F = \omega = 0$. This can be shown using the oscillation theorem (Goedbloed and Sakanaka 1974). The most unstable eigenfunction will have no internal node. When shear flow is included, and criterion (4.5) is satisfied, we still expect cluster spectra. However, when the marginal frequency $\tilde{\omega} = 0$ coincides with

a continuum frequency at some other position, the sequences of overstable cluster modes may disappear as in the case of clustering to the local extrema of the MHD continua (Bondeson et al. 1987).

The first term in (4.5) is the Rayleigh–Taylor term, which is destabilizing when $\rho' g > 0$ and $M^2 < 1$ and when $\rho' g < 0$ and $M^2 > 1$. The second term represents a correction due to compressibility. In the static case, the shear F' is stabilizing. However, with shear flow, the effect of shear is less clear-cut, owing to the appearance of F' in the shear Alfvén Mach number M. Note that the criterion blows up when $M^2 = M_c^2$ or $M^2 = 1$. As will be shown in Sec. 4.2, these points are associated with the transition from an ideal gravitational interchange cluster spectrum to a cluster spectrum associated with a local extremum of the slow or Alfvén continuum respectively.

4.2. Transition at the critical values of the shear flow

As mentioned in Sec. 4.1, (4.5) suggests that for values of M^2 slightly above M_c^2, the resonant surface is completely stable. However, as we shall see, at that moment a local extremum of the slow continuum will pass through the resonant layer where all four MHD continua coincide at the Doppler-shifted frequency $\omega = \mathbf{\Omega}_0$. This local extremum then takes over the overstable cluster spectrum of gravitational interchanges. See Bondeson et al. (1987) for the cylindrical case.

First, we calculate the position of the local extremum with respect to the resonant surface at $x = x_s$. Up to first order in $s = x - x_s$, we obtain for the static part of the slow continua

$$\omega_S \approx \frac{F' s}{\rho^{1/2}} M_c. \tag{4.6}$$

According to (3.2), the Doppler-shifted slow continua are given, up to second-order in s around the resonant surface, by

$$\mathbf{\Omega}_S^{\pm} \approx \mathbf{\Omega}_0 + \left(\mathbf{\Omega}_0' \pm M_c \frac{F'}{\rho^{1/2}} \right) s + \tfrac{1}{2} \mathbf{\Omega}_S^{\pm\prime\prime} s^2, \tag{4.7}$$

with derivative

$$\mathbf{\Omega}_S^{\pm\prime}(x) \approx -\frac{F'}{\rho^{1/2}} (M \mp M_c) + \mathbf{\Omega}_S^{\pm\prime\prime} s. \tag{4.8}$$

Here the definition (4.1) of the shear Alfvén Mach number has been used. Then, for $M \approx \pm M_c$, an extremum of $\mathbf{\Omega}_S^{\pm}$ occurs at the position $x_t = x_s + t$, where

$$t \approx \frac{F'}{\rho^{1/2}} \frac{M \mp M_c}{\mathbf{\Omega}_S^{\pm\prime\prime}}. \tag{4.9}$$

Here all quantities are evaluated at the resonant surface $x = x_s$.

Finally, we have to determine whether or not the extremum of the slow continuum can take over the cluster spectrum. As is mentioned in Sec. 3.4, the only possibility that cluster spectra will appear for small F, is at the minimum of $\mathbf{\Omega}_S^{+}$ (or maximum of $\mathbf{\Omega}_S^{-}$). Here (3.25) can be simplified to

$$\frac{k^2 \rho^2 g^2}{\gamma p + B^2} > \pm \tfrac{1}{4} \rho \omega_S \mathbf{\Omega}_S^{\pm\prime\prime} > 0. \tag{4.10}$$

Since ω_S is small, the first inequality is easily satisfied. However, by substituting

(4.6) and (4.9) into the second inequality, we obtain

$$\pm \tfrac{1}{4}\rho\omega_S\Omega_S^{\pm\prime\prime} = \pm\tfrac{1}{4}F'^2(M \mp M_c) > 0, \tag{4.11}$$

as the condition for the appearance of cluster spectra. Hence, for M slightly above M_c the cluster spectrum can be taken over by the local minimum of Ω_S^+. The same conclusion can be drawn for M slightly below $-M_c$ and the local maximum of Ω_S^-.

Proceeding to the analysis for the Alfvén continua along the same lines as for the slow continua, it can be shown that close to the critical shear Alfvén Mach number, $M^2 = 1$, a local extremum of either Ω_A^+ or Ω_A^- passes through the resonant surface. Moreover, the stability criterion for gravitational interchange modes is opposite to the criterion for clustering to the local extremum of the Alfvén continuum.

5. Numerical analysis of shear-flow cluster spectra

In this section, we present numerical results for the plane plasma slab with shear flow. First, the equilibrium model is discussed (Sec. 5.1). Then we look at the effect of shear flow on g-modes (Sec. 5.2), on stable Alfvén cluster spectra (Sec. 5.3), and finally on unstable interchange modes (Sec. 5.4).

5.1. Equilibrium model

We specialize to a force-free equilibrium, where the current density is proportional to the magnetic field,

$$\mathbf{j} \equiv \boldsymbol{\nabla} \times \mathbf{B} = \alpha\mathbf{B}, \tag{5.1}$$

and we take α to be constant. In components, (5.1) reads

$$B_y = \sin(\alpha x), \tag{5.2a}$$

$$B_z = \cos(\alpha x). \tag{5.2b}$$

To examine the effect of shear flow on g-modes, we take a linear flow profile (model A):

$$v_y = v_{y0}x, \qquad v_z = 0. \tag{5.3}$$

On the other hand, the criteria for the Alfvén cluster spectra, (3.22) and (3.22), contain the second-order derivative of the Alfvén continuum. In order to examine the effect of shear flow on clustering to the local extremum of the Alfvén continuum, we use a parabolic flow profile (model B):

$$v_y = 0, \qquad v_z = v_{z0}x^2. \tag{5.4}$$

For the other equilibrium profiles, we take

$$\rho = 1 + \rho_1 x, \tag{5.5a}$$

$$p = p_0 - g(x + \tfrac{1}{2}\rho_1 x^2), \tag{5.5b}$$

where the pressure is found from force balance, (2.6). Furthermore, we fix $\gamma = \frac{5}{3}$. According to Goedbloed and Dagazian (1971), the force-free equilibrium in slab geometry is completely stable against ideal instabilities in the absence of gravity and equilibrium flow. Here we shall look at the combined effect of both gravity and shear flow.

For the calculation of the linear MHD spectrum we used the finite-element code LEDAFLOW (see Nijboer et al. 1997). In this code, the eight MHD equations for the density ρ, the velocity $\mathbf{v}$, the temperature T and the magnetic field $\mathbf{B}$ are used.

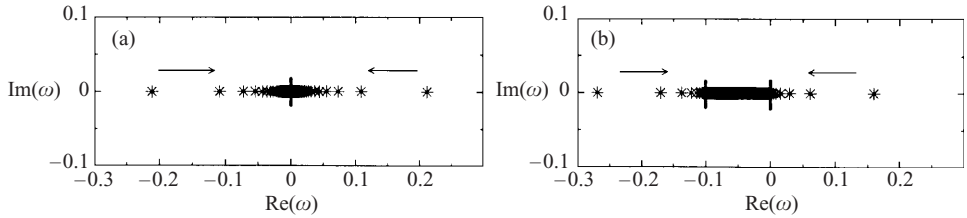

Figure 1. (a) Infinite sequences of discrete g-modes for the static case. (b) The effect of flow ($v_{y0} = -0.1$) on these waves. The arrows indicate the direction of the increasing number of nodes of the eigenmodes. The cluster point itself is marked by a vertical bar.

The pressure p is obtained from the ideal-gas law $p = \rho T$. The MHD equations are linearized by taking a $f(x)\exp(ik_y + ik_z - i\omega t)$ dependence for the perturbed Eulerian quantities. These quantities are then approximated by finite elements. The resulting eigenvalue problem is solved using standard eigenvalue solvers. The Lagrangian displacement vector $\boldsymbol{\xi}$ can be extracted from the perturbed Eulerian velocity (Frieman and Rotenberg 1960)

$$\mathbf{v}_1 = \frac{\partial \boldsymbol{\xi}}{\partial t} + \mathbf{v}\cdot\boldsymbol{\nabla}\boldsymbol{\xi} - \boldsymbol{\xi}\cdot\boldsymbol{\nabla}\mathbf{v}, \tag{5.6}$$

so that the relation $v_1 = -i\tilde{\omega}\xi$ holds for the x component.

5.2. g-modes

In Sec. 3.3, we considered the case of a gravitating plasma in the absence of magnetic shear such that $F = 0$ but with shear flow. It was pointed out there that, with the inclusion of gravity, the endpoints of the flow continuum $\boldsymbol{\Omega}_0(x)$ can induce cluster spectra of discrete modes. Here, we shall further investigate the spectral structure. For this purpose, the following parameters are choosen: $\rho_1 = -0.5$, $g = 1$, $p_0 = 2$, $\alpha = 0$, $k_y = 1$ and $k_z = 0$. This ensures that $\mathbf{k}\cdot\mathbf{B}$ is zero over the whole of the plasma domain. Furthermore, a linear flow profile (model A of Sec. 5.1) is used.

In Fig. 1, the resulting spectra are shown for the static case and for $v_{y0} = -0.1$. In the static case, two infinite sequences (in fact one sequence if we consider ω^2) of slow gravitational waves (g-modes) appear, accumulating to $\omega = 0$. However, if flow is included ($v_{y0} = -0.1$), we obtain a continuum, appearing in the real interval $[-0.1, 0]$ of ω and two infinite sequences of g-modes accumulating to both endpoints of this interval. For the given linear flow profile, these endpoints coincide with the boundary of the plasma. Figure 2 shows the eigenmode structures of the fifth cluster mode for both the static and flow case. These mode structures indicate that, for the flow case, these waves accumulate to the edge of the plasma.

5.3. Stable cluster spectra

In Sec. 3.4 it was mentioned that the local extrema of the MHD continua can induce cluster spectra. Stable cluster spectra can be constructed if the inhomogeneities are weak enough such that the frequencies of the local extrema do not coincide with other continua. By virtue of the set of inequalities (3.11), this is most easily accomplished for a local maximum of $\boldsymbol{\Omega}_A^+$ (or a minimum of $\boldsymbol{\Omega}_A^-$). In this section, we shall investigate the effect of shear flow on stable cluster spectra. For this purpose, we take $\rho_1 = 0.8$, $g = -10$, $\alpha = 0.5$, $p_0 = 0.5$ and $k_y = k_z = 1$ for the force-free equilibrium introduced in Sec. 5.1. With these parameters, $\rho' g$ will be negative,

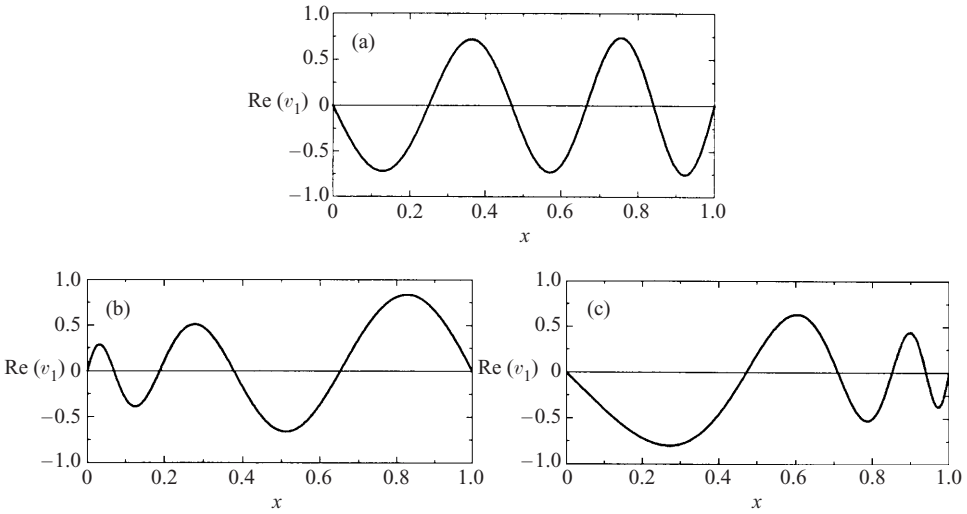

Figure 2. (a) The fifth cluster mode for the static case. (b,c) The effect of flow ($v_{y0} = -0.1$) on this mode, showing a localization at the boundary $x = 0$ (b) and at $x = 1$ (c).

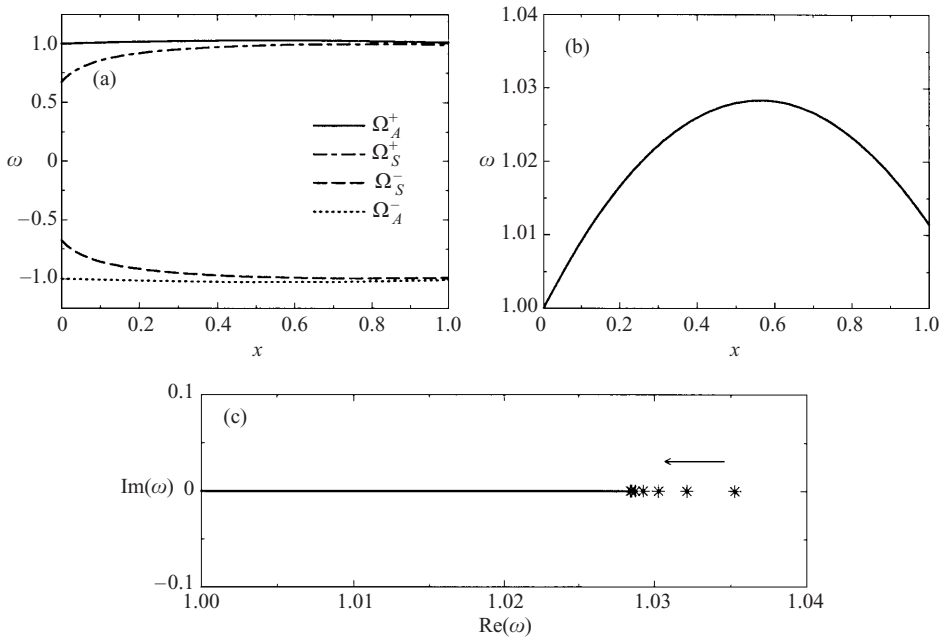

Figure 3. (a) The x dependence of the four continua for the static case ($v_{z0} = 0$). (b) The positive branch of the Alfvén continuum $\mathbf{\Omega}_A^+$. (c) The induced stable cluster spectrum. The arrow indicates the direction of the increasing number of nodes of the eigenmodes.

so that, according to (3.22) and (3.23), clustering to the local maximum of $\mathbf{\Omega}_A^+$ (the minimum of $\mathbf{\Omega}_A^-$) is possible, i.e. on the stable side of the Alfvén continua. Furthermore, as mentioned in Sec. 5.1, we take a parabolic flow profile (model B).

In Fig. 3, the four continua for the static case ($v_{z0} = 0$) are shown. The blow-up of the positive branch of the Alfvén continuum shows that there is a local maxi-

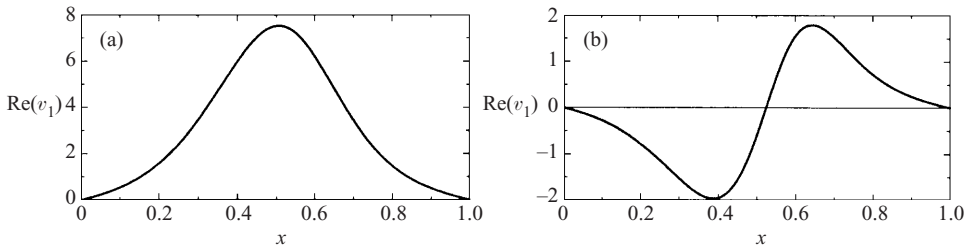

Figure 4. The first (a) and second (b) cluster modes.

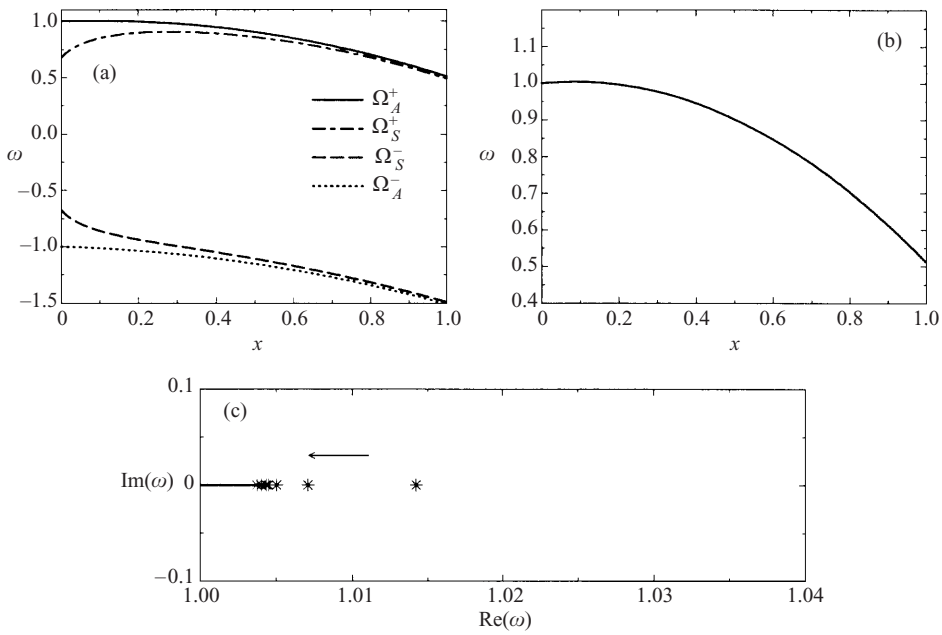

Figure 5. (a) The x dependence of the four continua with flow ($v_{z0} = -0.5$). (b) The positive branch of the Alfvén continuum $\mathbf{\Omega}_A^+$. (c) The induced stable cluster spectrum. The arrow indicates the direction of the increasing number of nodes of the eigenmodes.

mum. An infinite sequence of discrete modes, accumulating to the local maximum of the positive branch of the Alfvén continuum, is found. Of course, the same cluster modes appear at the negative branch of the Alfvén continuum, except for a sign reversal in the frequency. In Fig. 4, the eigenfunctions of the first two cluster modes of Fig. 3 are shown. In accordance with the oscillation theorem, the first eigenfunction contains no modes, and the second eigenfunction contains one node.

In Fig. 5, the cluster modes accumulating to the positive branch of the Alfvén continuum are shown with flow ($v_{z0} = -0.5$). Since the local maximum of $\mathbf{\Omega}_A^+$ does not coincide with continuum frequencies at other x positions, this cluster spectrum is stable. The eigenfunctions of the first two cluster modes are plotted in Fig. 6. Here the imaginary parts of these eigenfunctions are the same as the real parts. This is generally true when $\tilde{\omega}^2$ is real, because then the coefficients of (2.17) are real. Note that, as in the static case, the first eigenfunction contains no nodes, and the second

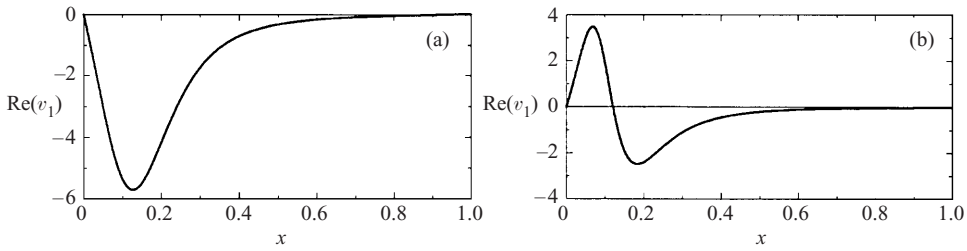

Figure 6. The first (a) and second (b) cluster modes.

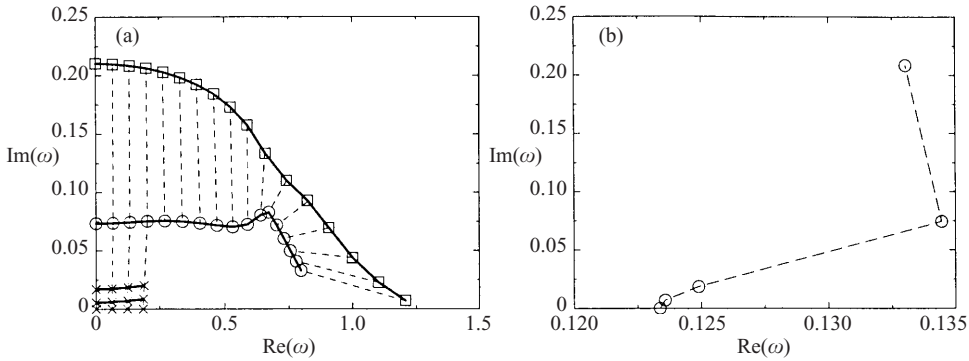

Figure 7. (a) First (squares) and second (circles) cluster mode frequencies for varying flow ($v_{z0} = 0, 0.1, \ldots, 1.6$). For $v_{z0} = 0, \ldots, 0.3$, the third, fourth and limiting frequencies (marked with $\times$) are also shown. (b) Blow-up of the cluster spectrum for $v_{z0} = 0.2$. For clarity the cluster modes are connected with dashed lines.

eigenfunction contains one node. There is no extremum of the negative branch of the Alfvén continuum, and no modes clustering to this branch were found.

5.4. Interchange modes

The interchange modes, described in Sec. 4, are also studied using the force-free equilibrium introduced in Sec. 5.1. Here we fix $k_y = 0$, $k_z = 1$ and $\alpha = 2$. With this choice of parameters, we have one resonant surface, $F = 0$ and $F' \neq 0$, situated at $x = \frac{1}{4}\pi$. Furthermore, we take $p_0 = 2.5$, $\rho_1 = 0.4$ and $g = 2$. For the flow profile, we again take the parabolic one (model B).

In Fig. 7, we have traced the first two cluster modes, starting with the static case ($v_{z0} = 0$). The same spectrum appears on the stable side ($\mathrm{Im}(\omega) < 0$). To determine the eigenvalues, we first used a QR solver to obtain a global picture of the spectrum, and then we used an inverse vector iteration for convergence. We could not follow the higher-order modes this way, however, since they are very local and need high resolution to determine.

Although (4.5) indicates stability for M^2 slightly larger than M_c^2 or 1 (since $\rho' g > 0$), corresponding to $v_{z0} \approx 0.81$ and 1.11, there are still unstable modes. However, as shown in Sec. 4.2, a local extremum of the slow magnetoacoustic or of the Alfvén continuum can pick up the sequence of instabilities. Note that the transitions are smooth for the first cluster mode, in the sense that the growth rate does not abruptly change. However, the second mode changes somewhat more around the critical shear Alfvén velocity. This mode is already more local, and

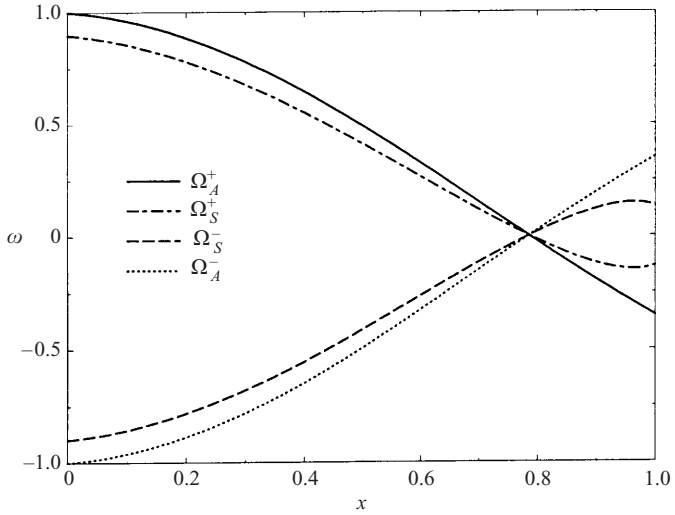

Figure 8. The x dependence of the four continua for the static case ($v_{z0} = 0$). The resonant surface is situated at $x = \frac{1}{4}\pi$.

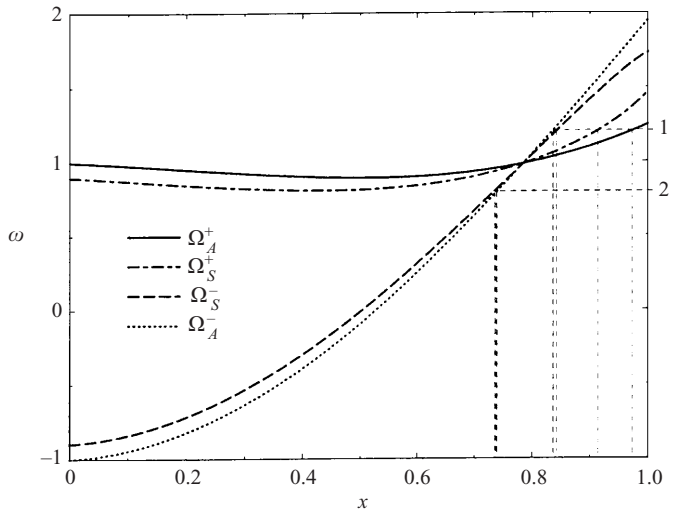

Figure 9. The x dependence of the four continua for the flow case ($v_{z0} = 1.6$). The labels '1' and '2' on the right-hand side indicate Re(ω) for the first and second cluster modes respectively.

therefore will notice the local changes in the equilibrium more than the first mode will.

In order to better understand why the growth rate of the first mode is smaller than that of the second mode for high velocities we have investigated their mode structure for the static case ($v_{z0} = 0$) and the flow case ($v_{z0} = 1.6$) and their relation to the continua. The four continua for the static case are shown in Fig. 8 and those for the flow case in Fig. 9. In both cases, the resonant surface is situated at $x = \frac{1}{4}\pi$. In Fig. 10, the first two unstable eigenfunctions are plotted for the static case. In accordance with the oscillation theorem, the first mode has no nodes

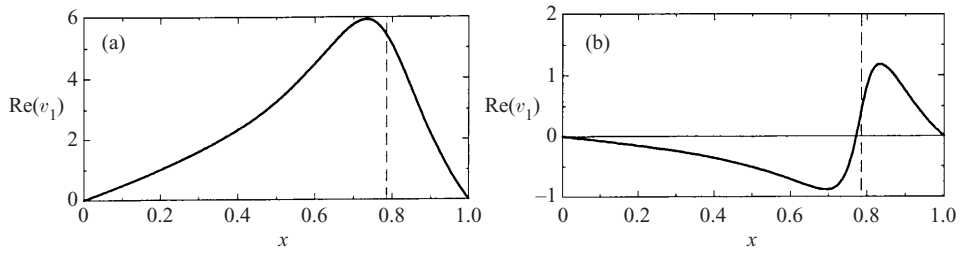

Figure 10. The first (a) and second (b) cluster modes for $v_{z0} = 0$. The dashed lines indicate the position of the $\mathbf{k} \cdot \mathbf{B} = 0$ surface.

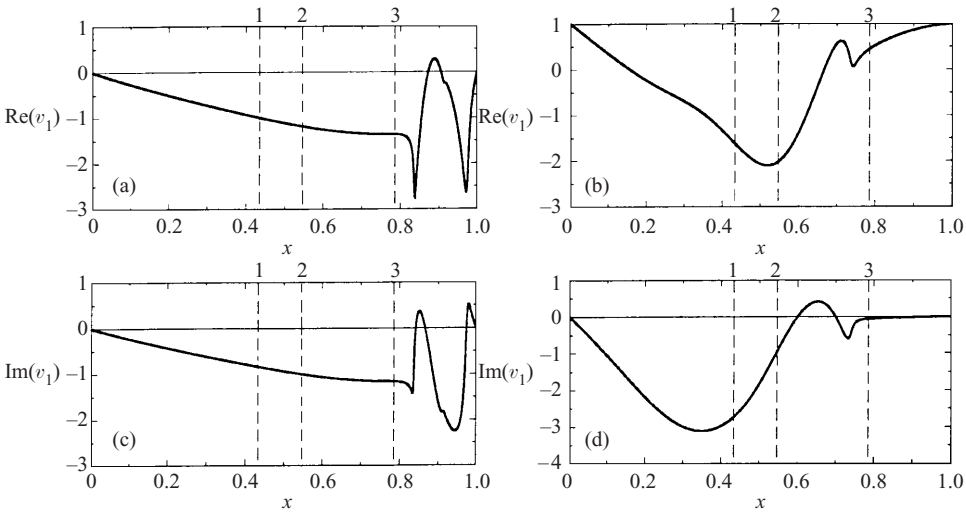

Figure 11. The first (a,c) and second (b,d) cluster modes for $v_{z0} = 1.6$. The labels '1', '2' and '3' on top indicate the positions of the local maximum of Ω_S^-, the local maximum of Ω_A^- and the $\mathbf{k} \cdot \mathbf{B} = 0$ surface respectively.

and the second mode has one node. In Fig. 11, the first two eigenfunctions are shown for $v_{z0} = 1.6$. Although for this flow parameter the criterion (4.5) indicates stability against gravitational interchanges, there are still unstable modes. Now these modes are induced by the minimum of the positive branch of the Alfvén and/or the slow continuum. The labels '1' and '2' on the right-hand side in Fig. 9 indicate the values of $\mathrm{Re}(\omega)$ for the first and second cluster modes for $v_{z0} = 1.6$, respectively. At the positions where these frequencies coincide with the continua, near-singular behaviour is found in the eigenfunctions. Since the first cluster mode is more singular than the second mode, it does look more like a continuum mode. Since continua are always stable in a plane slab, we may expect that this mode is indeed less unstable.

6. Conclusions

The ideal magnetohydrodynamic spectrum of gravitating plane plasmas with equilibrium flow has been investigated. It has been shown that infinite sequences of discrete modes may be induced at the resonant surface or by a local extremum of

the Alfvén or slow continuum. The criteria for these modes to appear have been derived. Furthermore, it has been shown that, above certain critical values of the shear flow at a resonant surface, the overstable gravitational interchanges may disappear. However, at these critical values, a local extremum of either the slow or the Alfvén continuum is passing through the resonant layer. These extrema can then take over the infinite sequences of overstable modes. It has been shown numerically that shear flow decreases the growth rate of the overstable gravitating interchange modes. However, around the above-mentioned critical values of the shear flow, the growth rates of the higher-order modes may increase.

Finally, the classical flow continua in hydrodynamics are extended with compressibility. When gravity is included, the endpoints of the flow continua can be cluster points of discrete spectra outside the flow continuum.

Acknowledgements

This work was performed as part of the research program of the association agreement of Euratom and the Stichting voor Fundamenteel Onderzoek der Materie (FOM), with financial support from the Nederlandse Organisatie voor Wetenschappelijk Onderzoek (NWO) and Euratom.

References

Appert, K., Gruber, R. and Václavík, J. 1974 Continuous spectra of cylindrical magnetohydrodynamic equilibrium. *Phys. Fluids* **17**, 1471–1472.

Berge, G. 1997 A Lyapunov functional for stability of ideal magnetohydrodynamic systems in arbitrary motion. *Phys. Plasmas* **4**, 1201–1212.

Bondeson, A., Iacono, R. and Bhattacharjee, A. 1987 Local magnetohydrodynamic instabilities of cylindrical plasma with sheared equilibrium flows. *Phys. Fluids* **30**, 2167–2180.

Case, K. M. 1960a Stability of inviscid plane Couette flow. *Phys. Fluids* **3**, 143–148.

Case, K. M. 1960b Stability of an idealized atmosphere. I. Discussion of results. *Phys. Fluids* **3**, 149–154.

Chu, M. S., Greene, J. M., Jensen, T. H., Miller, R. L., Bondeson, A., Johnson, R. W. and Mauel, M. E. 1995 Effect of toroidal plasma flow and flow shear on global magnetohydrodynamic MHD modes. *Phys. Plasmas* **2**, 2236–2241.

Corbelli, E. and Torricelli-Ciamponi, G. 1989 Stability of magnetohydrodynamic cylindrical flows: compressible modes. *Phys. Fluids* **B2**, 828-836.

Dyson, F. J. 1960 Stability of an idealized atmosphere. II. Zeros of the confluent hypergeometric function. *Phys. Fluids* **3**, 155–157.

Frieman, E. and Rotenberg, M. 1960 On hydromagnetic stability of stationary equilibria. *Rev. Mod. Phys.* **32**, 898–902.

Goedbloed, J. P. 1971 Stabilization of magnetohydrodynamic instabilities by force-free fields. *Physica* **53**, 412–444.

Goedbloed, J. P. 1974 Unpublished memorandum, Courant Institute.

Goedbloed, J. P. 1984 Plasma–vacuum interface problems in magnetohydrodynamics. *Physica* **12D**, 107–132.

Goedbloed, J. P. 1998 Once more: the continuous spectrum of ideal magnetohydrodynamics. *Phys. Plasmas* **5**, 3143–3154.

Goedbloed, J. P. and Dagazian, R. Y. 1971 Kinks and tearing modes in simple configurations. *Phys. Rev.* **A4**, 1554.

Goedbloed, J. P. and Sakanaka, P. H. 1974 New approach to magnetohydrodynamic stability. *Phys. Fluids* **17**, 918.

Goedbloed, J. P., van der Holst, B. and Keppens, R. 1999 To be published.

Gonzáles, A. G. and Gratton, J. 1994 The Kelvin–Helmholtz instability in a compressible plasma: the role of the orientation of the magnetic field with respect to the flow. *J. Plasma Phys.* **51**, 43–60.

Grad, H. 1973 Magnetofluid-dynamic spectrum and low shear stability. *Proc. Natl. Acad. Sci. USA* **70**, 3277–3281.

Hameiri, E. 1981 Spectral estimates, stability conditions, and the rotating screw-pinch. *J. Math. Phys.* **22**, 2080–2088.

Miura, A. and Pritchett, P. L. 1982 Nonlocal stability analysis of the MHD Kelvin–Helmholtz instability in a compressible plasma. *J. Geophys. Res.* **87**, 7431–7444.

Newcomb, W. E. 1960 Hydromagnetic stability of a diffuse linear pinch. *Ann. Phys. (NY)* **10**, 232–267.

Newcomb, W. E. 1961 Convective instability induced by gravity in a plasma with a frozen-in magnetic field. *Phys. Fluids* **4**, 391–396.

Nijboer, R. J., van der Holst, B., Poedts, S. and Goedbloed, J. P. 1997 Calculating magnetohydrodynamic flow spectra. *Comput. Phys. Commun.* **106**, 39–52.

Suydam, B. R. 1959 Stability of a linear pinch. In: *Proceedings of 2nd UN International Conference on Peaceful uses of Atomic Energy*, Vol. 31, p. 157. Columbia University Press, New York.